Hindawi Publishing Corporation
Mathematical Problems in Engineering
Volume 2009, Article ID 693081, 13 pages
doi:10.1155/2009/693081

Research Article

Flux Reflection Model of the Ferroresonant Circuit

Kruno Miličević, Ivan Flegar, and Denis Pelin

Faculty of Electrical Engineering, University of Osijek, Kneza Trpimira 2b, 31000 Osijek, Croatia

Correspondence should be addressed to Kruno Miličević, kruno.milicevic@etfos.hr

Received 10 March 2009; Revised 20 May 2009; Accepted 5 June 2009

Recommended by José Roberto Castilho Piqueira

The paper presents a linear model of ferroresonant circuit with flux reflection. The proposed model—flux reflection model—derives from observations of typical flux waveforms of nonlinear coil during ferroresonant steady states. Simulation results of the flux reflection model are compared with simulation results of the usual nonlinear model as well as with measurements carried out on the physical model of the ferroresonant circuit. The flux reflection model enables a novel comprehension of the ferroresonant circuit behavior and simplifies the modeling of the nonlinear coil in the ferroresonant circuit.

1. Introduction

A ferroresonant circuit is a circuit which comprises a linear capacitor in series with a nonlinear coil, driven by a sine-wave voltage. The ferroresonant circuit can exhibit several bifurcations and a chaotic steady state [1–5]. Common research procedures comprise the measurements of ferroresonant circuit and the computer simulation of the mathematical model based on state-equations of the circuit.

The nonlinearity of the model caused by the nonlinear magnetization characteristic of the coil is the driving force on the route to the chaotic steady state, which is marked by the bifurcations that are initiated by varying values of a circuit parameter. Complex models, that comprehend more nonlinear elements, are needed to match results of measurements and simulation completely [6, 7]. In order to obtain the complex behavior of the circuit, the nonlinear element that comprises the magnetization nonlinearity is only necessary. Therefore, the model comprises the magnetization nonlinearity $i_L(\varphi)$, implying the core saturation of the coil. The winding resistance of the coil is neglected, and the resistor, that represents the core losses of the coil, is assumed to be linear. State equations of the ferroresonant circuit, Figure 1, are

$$\frac{d\varphi}{dt} = u_L = \widehat{U}\sin\omega t - u_C,$$

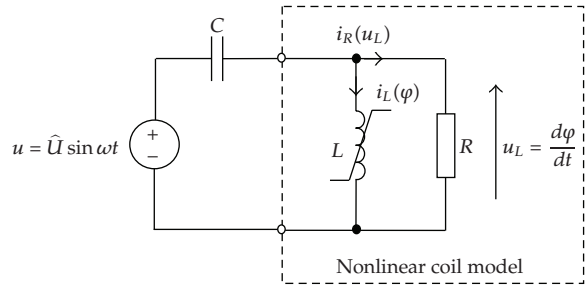

Figure 1: Ferroresonant circuit.

$$\frac{du_C}{dt} = \frac{1}{C}\left[\frac{1}{R}\left(\widehat{U}\sin\omega t - u_C\right) + i_L(\varphi)\right]. \tag{1.1}$$

The magnetization nonlinearity $i_L(\varphi)$ is odd-symmetric and monotonically increasing. It can be presented in various forms, for example, in a polynomial form [8, 9] or piecewise linear form [10, 11]. Thereby, the polynomial form is obtained often by an interpolation of a piecewise linear form. The magnetization nonlinearity is based on measurements carried out on a nonlinear coil regarding the above-mentioned assumptions made about properties of the coil. For example, one ought to rely on the results of standard measurements carried out on the nonlinear coil by the manufacturer [11, 12]. Because of a limited thermal endurance of the coil, measurements cannot be carried out by applying the sine-wave voltage for the full range of flux and voltage peak values which occur in some operation modes of ferroresonant circuit. However, the importance of this problem is often ignored by a simple extrapolation of magnetization nonlinearity obtained by measurements.

Further problem of modeling based on standard measurements is that the parameters of model depend on the number of measurements, that is, on the number of measured values on *U-I* characteristic. Namely, a piecewise linear form of the magnetization nonlinearity, that is obtained by a small number of measurements, would not be as smooth as necessary; in the case of polynomial form of the magnetization nonlinearity, a small number of measurements could result with a significant interpolation error.

In the paper a novel kind of modeling the magnetization characteristic of the coil in the ferroresonant circuit is presented. The modeling will be based on a characteristic behavior that nonlinear coil exhibits in a ferroresonant circuit. The behavior will be identified from the flux waveforms obtained by measurements and by computer simulation.

The preliminary purpose of obtained novel model of the ferroresonant circuit is to enable a new comprehension of the circuit behavior and to simplify the modeling of nonlinear coil in the ferroresonant circuit by reducing the number of model parameters.

2. Measurements and Nonlinear Model

In order to notice the characteristic behavior of a coil in ferroresonant circuit, the ferroresonant steady states are obtained by measurements carried out on a ferroresonant circuit that is realized in laboratory and by computer simulation carried out on a typical nonlinear model of the ferroresonant circuit.

The ferroresonant circuit realized in the laboratory is composed of the capacitor $C = 20\,\mu F$ and the primary winding of the toroidal iron-cored two-windings transformer used as a nonlinear coil. The transformer was designed for the nominal apparent power of 200 VA and for the nominal primary voltage of 30 V. The core is strip-wounded, made of Ni-Fe alloy (Trafoperm N3). The autotransformer of 10 kVA nominal apparent power is used as a variable voltage source in all experiments.

To simplify calculations, throughout the rest of the paper all the variables and parameters of the ferroresonant circuit are expressed in relation to reference quantities, that is, in a per-unit system:

$$\overline{\varphi} = \varphi \frac{\omega}{U_{\text{ref}}}, \qquad \overline{u}_C = \frac{u_C}{U_{\text{ref}}}, \qquad \overline{\omega} = \frac{\omega}{\omega_{\text{ref}}}, \qquad \overline{i}_L = \frac{i_L}{I_{\text{ref}}}, \qquad \overline{\widehat{U}} = \frac{\widehat{U}}{U_{\text{ref}}}, \tag{2.1}$$
$$U_{\text{ref}} = 31.2\,\text{V}, \qquad I_{\text{ref}} = 0.19\,\text{A}, \qquad \omega_{\text{ref}} = 314\,\text{s}^{-1}.$$

The simulation is carried out using a typical nonlinear model of ferroresonant circuit, with the polynomial form of magnetization nonlinearity:

$$\frac{d\overline{\varphi}}{dt} = \overline{u}_L = \overline{\widehat{U}} \sin \overline{\omega} t - \overline{u}_C,$$
$$\frac{d\overline{u}_C}{dt} = \frac{1}{\overline{C}} \left[\frac{1}{\overline{R}} \left(\overline{\widehat{U}} \sin \overline{\omega} t - \overline{u}_C \right) + i_L(\overline{\varphi}) \right], \tag{2.2a}$$
$$\overline{\omega} = 1, \qquad \overline{C} = 1,$$
$$\overline{i}_L(\overline{\varphi}) = f(\overline{\varphi}) \operatorname{sign}(\overline{\varphi}),$$
$$f(\overline{\varphi}) = \sqrt{0.034 \cdot \overline{\varphi}^2 + 5.54 \cdot 10^{-3} \cdot \overline{\varphi}^{20} + 1.05 \cdot 10^{-5} \cdot \overline{\varphi}^{38}}, \tag{2.2b}$$
$$\overline{R} = 2.$$

The magnetization characteristic $\overline{i}_L(\overline{\varphi})$ and the iron-core losses $\overline{R}$ are derived from measured *P-U* and *U-I* characteristic of the nonlinear coil [12].

During measurements and simulation the steady states are obtained by varying the amplitude $\overline{\widehat{U}}$ of source voltage within the range:

$$0 < \overline{\widehat{U}} \leq 3. \tag{2.3}$$

The step of the amplitude variation is $\Delta\overline{\widehat{U}} = 0.05$ in simulation, as well as in measurements. Simulation is carried out by using the 4th order Runge-Kutta method with 10000 integration steps per period, $j = 1, \ldots, 10000$.

Characteristic steady states and bifurcations obtained by simulation and measurements are shown in Tables 1 and 2, respectively. There is no significant disagreement between results of simulation and measurements with the exception of the pitchfork bifurcation and the period-four steady state, which are not noticed in measurements.

Table 1: Steady states and *bifurcations* of the nonlinear model of ferroresonant circuit obtained by simulation.

Increasing $\widehat{\mathrm{U}}$	Decreasing $\widehat{\mathrm{U}}$	Steady states and bifurcations
$0 < \widehat{U} < 1.05$	$0 < \widehat{U} < 0.75$	Monoharmonic steady state
$\widehat{U} = 1.05$	—	*Forward ferroresonant jump*
—	$\widehat{U} = 0.75$	*Reverse ferroresonant jump*
$1.05 \leq \widehat{U} < 1.7$	$0.75 \leq \widehat{U} < 1.7$	Odd higher harmonic steady state
$\widehat{U} = 1.7$		*Pitchfork bifurcation*
$1.7 \leq \widehat{U} < 2.4$		Even and odd higher harmonic steady state
$\widehat{U} = 2.4$		*Period-doubling bifurcation*
$2.4 \leq \widehat{U} < 2.55$		Period-two steady state
$\widehat{U} = 2.55$		*Period-doubling bifurcation*
$2.55 \leq \widehat{U} < 2.65$		Period-four steady state
$2.65 < \widehat{U} < 3$		Chaotic steady state

Table 2: Steady states and *bifurcations* of the ferroresonant circuit realized in the laboratory obtained by measurements.

Increasing $\widehat{U}$	Decreasing $\widehat{U}$	Steady states and bifurcations
$0 < \widehat{U} < 1$	$0 < \widehat{U} < 0.7$	Monoharmonic steady state
$\widehat{U} = 1$	—	*Forward ferroresonant jump*
—	$\widehat{U} = 0.7$	*Reverse ferroresonant jump*
$1 \leq \widehat{U} < 1.4$	$0.7 \leq \widehat{U} < 1.4$	Odd higher harmonic steady state
$\widehat{U} = 1.4$		*Pitchfork bifurcation*
$1.7 \leq \widehat{U} < 2.2$		Even and odd higher harmonic steady state
$\widehat{U} = 2.2$		*Period-doubling bifurcation*
$2.2 \leq \widehat{U} < 2.6$		Period-two steady state
Not obtained		*Period-doubling bifurcation*
		Period-four steady state
$2.6 < \widehat{U} < 3$		Chaotic steady state

By that means, Figure 3 implies that the peak value of flux $\widehat{\overline{\Phi}}$ is in all polyharmonic steady states limited by the value $\overline{\Phi}_{\mathrm{sat}} \approx 1.5$, called here as a flux saturation value:

$$|\varphi| \leq \overline{\Phi}_{\mathrm{sat}}. \tag{2.4}$$

From simulation as well as measurements it is observed that during all steady states the slope of flux, immediately before and after the moment each time the flux reaches the peak value $\widehat{\overline{\Phi}}$, changes the sign only, that is, holding the same absolute value nearly. As it is seen in Figure 2, for instance, at the moment t_1, we assume

$$\left.\frac{d\overline{\varphi}}{dt}\right|_{t_1-0} \approx -\left.\frac{d\overline{\varphi}}{dt}\right|_{t_1+0}. \tag{2.5}$$

This property is named here as a flux reflection.

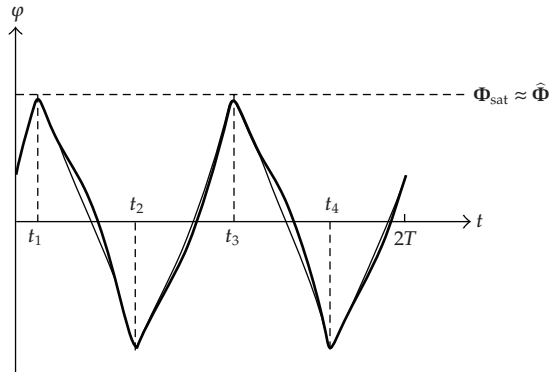

Figure 2: Typical ferroresonant steady state waveform of flux obtained by measurements (bold line) and simulation (thin line) for source voltage amplitude $\widehat{\overline{U}} = 1.1$.

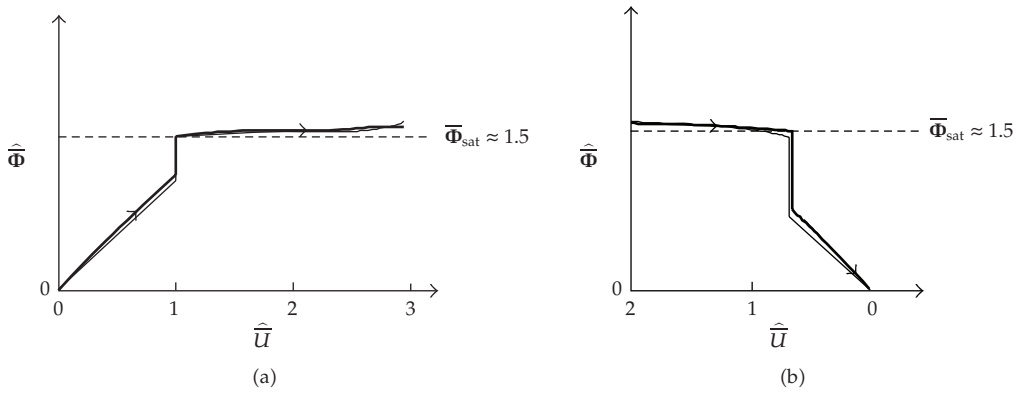

Figure 3: Peak values of flux obtained by measurements (bold line) and by computer simulation (thin line): (a) by increasing the source voltage amplitude $\widehat{\overline{U}}$, (b) by decreasing the source voltage amplitude $\widehat{\overline{U}}$.

3. Flux Reflection Model

Novel presentation of magnetization nonlinearity is based on observed limitation (2.4) and reflection (2.5) of flux values. Thereby, the magnetization characteristic for values $|\varphi| < \overline{\Phi}_{\text{sat}}$ is approximated by a linear inductance $\overline{i}_L(\overline{\varphi}) \approx (1/\overline{L})\overline{\varphi}$. In a case of the polynomial form of magnetization nonlinearity (2.2b) the linear inductance $\overline{L} = 5.4$ is approximated as shown on Figure 4.

By the reducing of the nonlinear magnetization characteristic to the linear inductance $\overline{L}$, the state-equations of the ferroresonant circuit, (2.2a) and (2.2b), become linear between two flux reflections, that is, for flux values $|\varphi| < \overline{\Phi}_{\text{sat}}$:

$$\begin{aligned} \frac{d\overline{\varphi}}{dt} &= \overline{u}_L = \widehat{\overline{U}} \sin \overline{\omega} t - \overline{u}_C, \\ \frac{d\overline{u}_C}{dt} &= \frac{1}{\overline{C}} \left[\frac{1}{\overline{R}} \left(\widehat{\overline{U}} \sin \overline{\omega} t - \overline{u}_C \right) + \frac{1}{\overline{L}} \overline{\varphi} \right], \\ \overline{\omega} &= 1, \quad \overline{C} = 1, \quad \overline{R} = 2, \quad \overline{L} = 5.4. \end{aligned} \tag{3.1}$$

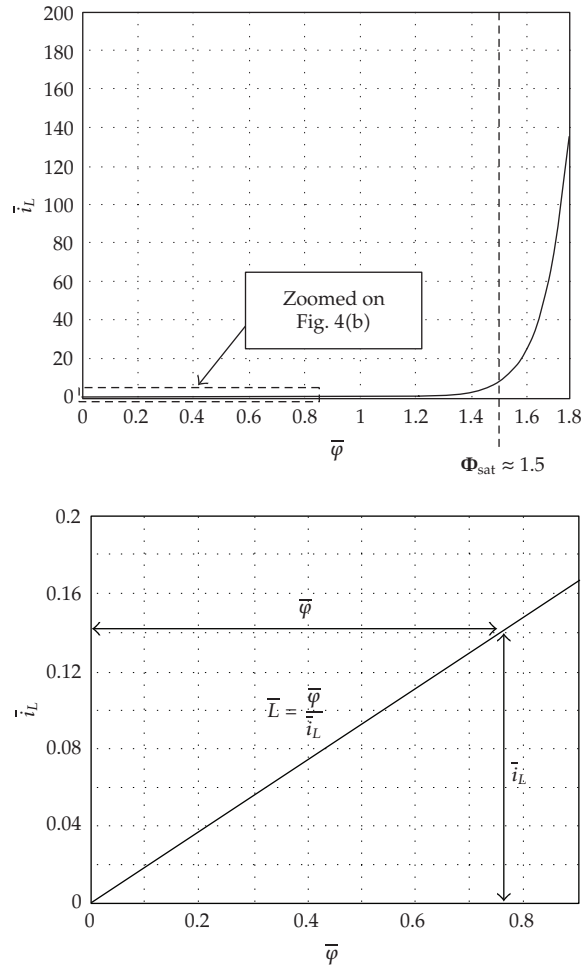

Figure 4: (a) Polynomial form of the magnetization nonlinearity. (b) Zoomed linear part of the magnetization nonlinearity.

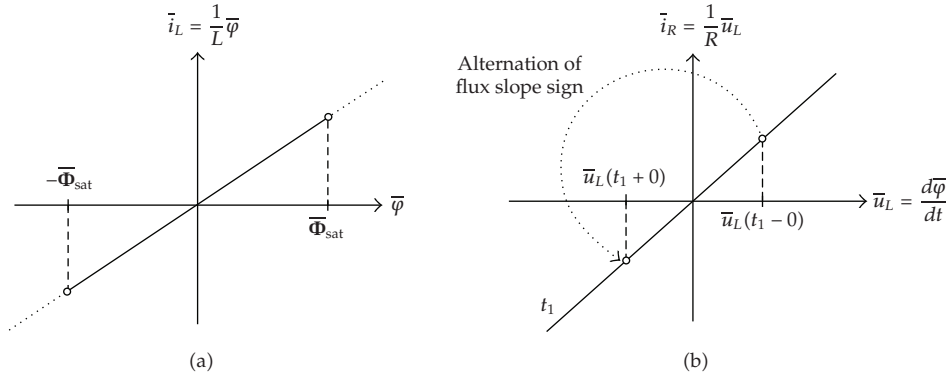

Figure 5: Magnetization characteristic $\bar{i}_L(\overline{\varphi})$ of the flux reflection model and the alternation of flux slope sign shown on $\bar{i}_R(\overline{u}_L)$ characteristic.

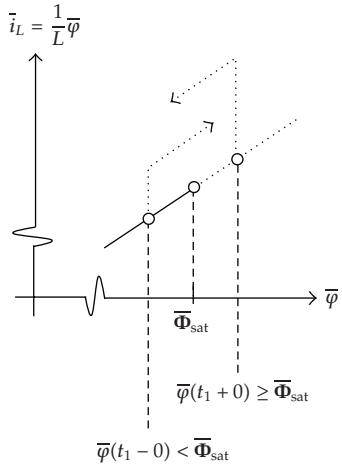

Figure 6: Part of the magnetization characteristic zoomed near the saturation value $\bar{\Phi}_{sat}$.

Thereby, the observed properties of a ferroresonant circuit—the limitation of flux values (2.4) and the flux reflection (2.5)—can be realized easily, using the following pseudocode:

$$\begin{aligned}
&FOR\ each\ integration\ step\ j\\
&\quad calculate\ \left.\frac{d\bar{\varphi}}{dt}\right|_{j+1}\ as\ defined\ by\ used\ iterative\ method\\
&\quad IF\ \left|\bar{\varphi}(j)\right| > \bar{\Phi}_{sat}\ THEN\\
&\qquad set\ \left.\frac{d\bar{\varphi}}{dt}\right|_{j+1}\ to\ be\ equal\ to\ -\left.\frac{d\bar{\varphi}}{dt}\right|_{j}\\
&\quad END\ IF\\
&END\ FOR
\end{aligned} \tag{3.2}$$

The proposed flux reflection model, defined by state-equations (3.1) and pseudocode (3.2), could be comprehended as a piecewise linear model also. However, contrary to a typical piecewise linear model, this model comprises only one set of state-equations, that is, the magnetization characteristic $\bar{i}_L(\bar{\varphi})$ with only one linear segment. As it is shown on Figures 5 and 6 and determined by the pseudocode (3.2), the segment is limited by the saturation value $\bar{\Phi}_{sat}$ which triggers the alternation of flux slope sign and, at this way, causes the change of flux trend. For instance, the open arrows on Figure 6 indicate the increasing of flux value before the flux reflection and the decreasing of flux values after the flux reflection. Figures 5 and 6 show the flux reflection for the case $\bar{\varphi} \geq \bar{\Phi}_{sat}$ only. The depiction of the flux reflection for the case $\bar{\varphi} \leq -\bar{\Phi}_{sat}$ can be derived from the mirror symmetry of flux reflection model easily.

Table 3: Steady states and *bifurcations* of the flux reflection model of ferroresonant circuit.

Increasing $\widehat{\overline{U}}$	Decreasing $\widehat{\overline{U}}$	Steady states and bifurcations
$0 < \widehat{\overline{U}} < 1.15$	$0 < \widehat{\overline{U}} < 0.8$	Monoharmonic steady state, Figure 7(a)
$\widehat{\overline{U}} = 1.15$	—	*Forward ferroresonant jump*
—	$\widehat{\overline{U}} = 0.8$	*Reverse ferroresonant jump*
$1.15 \leq \widehat{\overline{U}} < 1.7$	$0.8 \leq \widehat{\overline{U}} < 1.7$	Odd higher harmonic steady state, Figure 7(b)
$\widehat{\overline{U}} = 1.7$		*Pitchfork bifurcation*
$1.7 \leq \widehat{\overline{U}} < 2.25$		Even and odd higher harmonic steady state, Figure 7(c)
Not obtained		*Period-doubling bifurcation* Period-two steady state *Period-doubling bifurcation* Period-four steady state
$2.25 \leq \widehat{\overline{U}} \leq 3$		Chaotic steady state, Figure 7(d)

4. Comparison of the Flux Reflection Model and the Nonlinear Model

The flux reflection model can be considered as a model of the ferroresonant circuit only if the flux reflection model reveals a complex behavior of the ferroresonant circuit. Therefore, the steady states of the flux reflection model are obtained in the same way as for the ferroresonant circuit realized in laboratory and for the nonlinear model in Section 2, that is, by varying the amplitude $\widehat{\overline{U}}$ with the step of the amplitude variation $\Delta\widehat{\overline{U}} = 0.05$ within a range:

$$0 < \widehat{\overline{U}} \leq 3. \tag{4.1}$$

Between two flux reflections the flux reflection model is described by linear state equations (3.1). Thus, these equations can be solved analytically. However, as it is shown in the appendix in detail, at the start of transient state, that is, in moment $t = 0$, it is not possible to determine explicitly the ranges of parameter values and values of initial conditions at which a particular steady state would arise; it is only possible to solve (3.1) for a given set of parameter values and values of initial conditions.

In the paper the steady states solutions are obtained in the same way as for the nonlinear model in Section 2, that is, by simulation that is carried out numerically, using the 4th order Runge-Kutta method with 10000 integration steps per period, $j = 1, \ldots, 10000$.

The route to the chaotic steady state with bifurcations and corresponding steady states is obtained by varying the source voltage amplitude $\widehat{\overline{U}}$, (3.1), as shown on Table 3. Figure 7 shows the flux waveforms corresponding to each of steady states of the flux reflection model shown in Table 3.

The results of simulation based on the nonlinear model and results of measurements, shown on Tables 1 and 2, differ from results of simulation based on the flux reflection model shown on Table 3. For instance, the period-two steady state as well as period-four steady state and corresponding period-doubling bifurcations, are not obtained by simulation based on flux reflection model. The reason for this could be the approximation of the maximum value of flux by a constant saturation value $\overline{\Phi}_{\text{sat}}$. Namely, on Figure 3 during the polyharmonic steady states the maximum value of flux is constant only nearly, that is, it is not equal to the chosen saturation value ($\overline{\Phi}_{\text{sat}} = 1.5$).

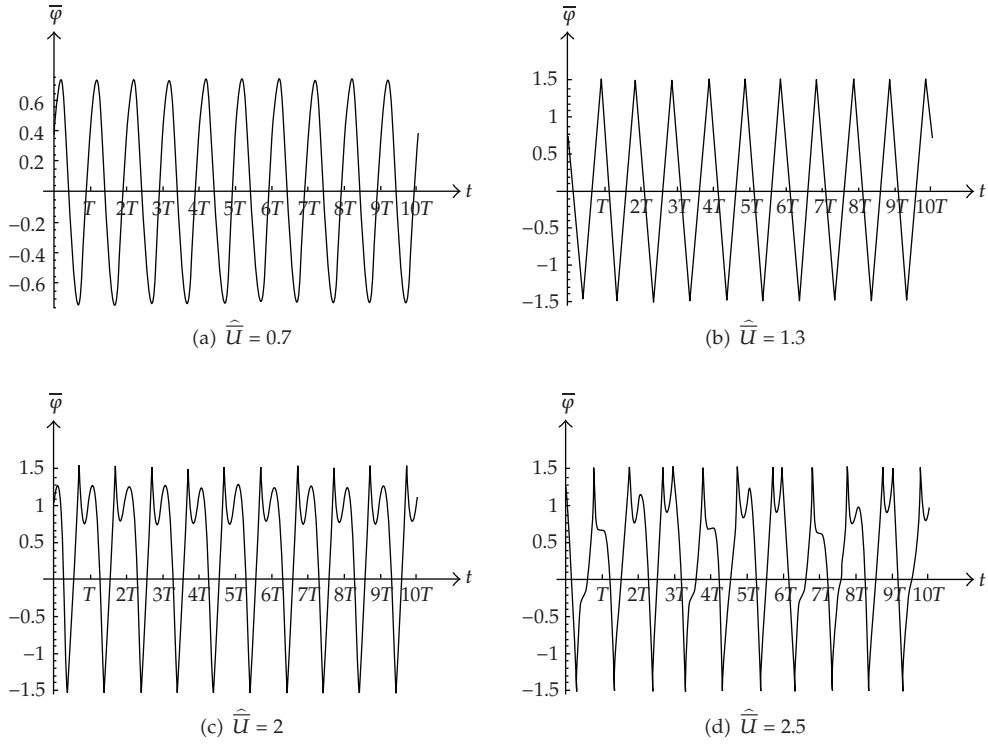

Figure 7: Flux waveforms of the flux reflection model: (a) monoharmonic steady state, (b) odd higher harmonic steady state, (c) even and odd higher harmonic steady state, and (d) chaotic steady state.

The main shortcoming of the flux reflection model is the inherent limitation of inductive component of the coil current $\overline{i}_L$

$$\left|\overline{i}_L(t)\right| \leq \left|\overline{i}_L\left[\overline{\varphi}(t_1+0)\right]\right| \approx \left|\overline{i}_L\left(\overline{\Phi}_{\text{sat}}\right)\right| = \left|\frac{1}{\overline{L}}\overline{\Phi}_{\text{sat}}\right| \tag{4.2}$$

which does not exist in the actual ferroresonant circuit.

In spite of that, the proposed model reveals a complex steady state behavior of the ferroresonant circuit. Besides of a new comprehension of the circuit behavior, the flux reflection model enables a simple modeling of the nonlinear coil. It is sufficient to carry out the simple measurements to determine the value of linear inductance L and the saturation value Φ_{sat}.

5. Additional Simulation

The additional simulation is carried out in order to investigate the sensitivity of flux reflection model on the value of linear inductance L and on the saturation value Φ_{sat}. The step of the source voltage amplitude variation is $\Delta\widehat{\overline{U}} = 0.05$. Simulation is carried out by using the 4th order Runge-Kutta method with 10000 integration steps per period.

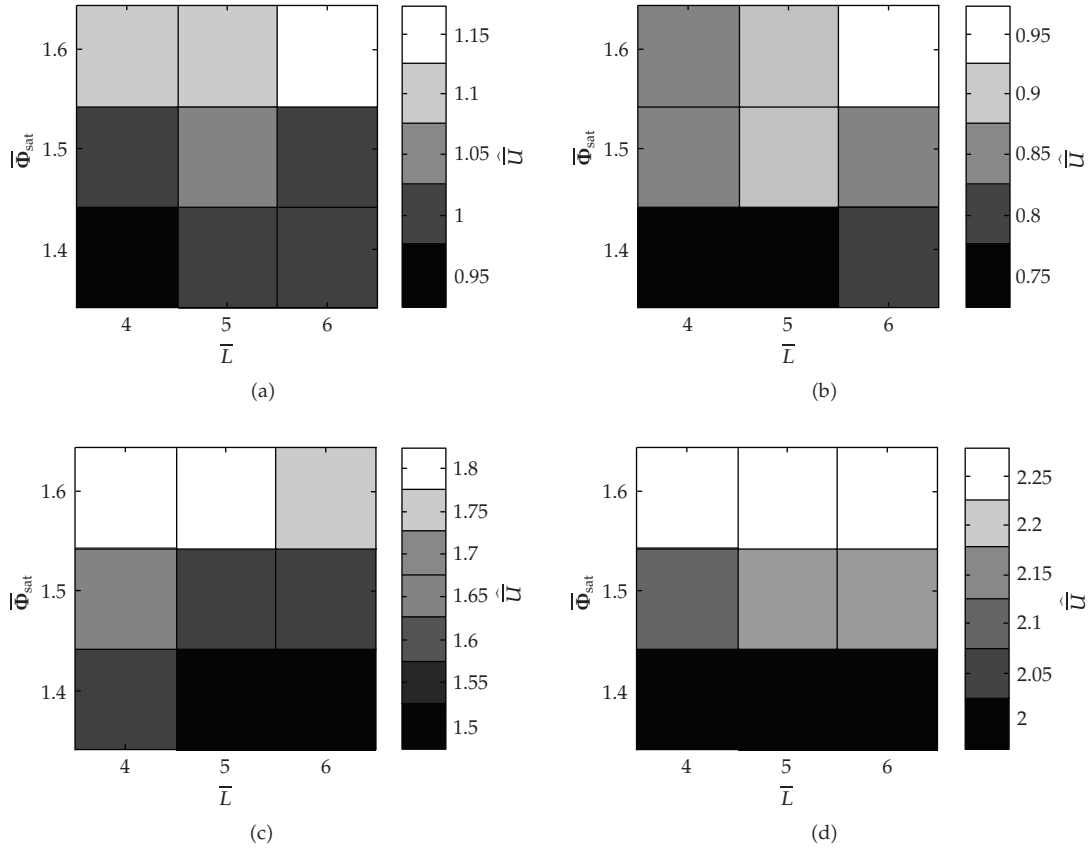

Figure 8: Influence of saturation value Φ_{sat} and linear inductance L on the initiation of (a) forward ferroresonant jump, (b) reverse ferroresonant jump, (c) pitchfork bifurcation, and (d) chaotic steady state.

Figure 8 shows results of simulation. For easier visualisation the diagrams are constructed using gray scaled squares where different shades of gray are employed to represent values of source voltage amplitude $\widehat{\overline{U}}$ at which the particular bifurcation and steady state, respectively, has occurred. For instance, the bottom left square on Figure 8(c) (■) indicates that the pitchfork bifurcation for the parameter values $\overline{\Phi}_{sat} = 1.4$, $\overline{L} = 4$, occur at the source voltage amplitude $\widehat{\overline{U}} = 1.55$.

The results of simulation reveal that the flux reflection model is more sensitive to the variation of the saturation value Φ_{sat}, than to the value of linear inductance L. For instance, for the saturation value $\overline{\Phi}_{sat} = 1.4$ and linear inductance values $\overline{L} = 4, 5, 6$, the reverse ferroresonant jump occurs at the source voltage amplitude values $\widehat{\overline{U}} = 0.85$ (■) and $\widehat{\overline{U}} = 0.90$ (■), as it is presented by middle row on Figure 8(b). For the linear inductance value $\overline{L} = 5$ and the saturation values $\overline{\Phi}_{sat} = 1.4; 1.5; 1.6$, the reverse ferroresonant jump occurs for a wider range of source voltage amplitude values, $\widehat{\overline{U}} = 0.75$ (■) and $\widehat{\overline{U}} = 0.90$ (■), as it is presented by middle column on Figure 8(b).

Therefore, it is more important to know the saturation value Φ_{sat}precisely than the value of linear inductance L.

6. Conclusions

The flux reflection model preserves the basic properties of the magnetization characteristic: linearity and saturation. Despite the noticed shortcomings, the flux reflection model reveals a complex steady state behavior characteristic for the ferroresonant circuit. It enables a new comprehension of the behavior of the ferroresonant circuit and simplifies the modeling of the nonlinear coil in the ferroresonant circuit.

Future work will address the simplification of the identification of parameters of a flux reflection model in order to avoid the identification by using the waveforms of flux values during ferroresonant steady states. Namely, in a flux reflection model a coil is defined by a linear inductance value and by a saturation value, which could be determined by standard measurements experimentally or by number of windings and by core parameters of coil analytically.

Furthermore, in order to expand the purpose of the model from the presented new comprehension of the circuit behavior to a wide application of the model, it will be necessary to identify advantages and disadvantages of the flux reflection model precisely by a more detailed comparison with usual models of ferroresonant circuit.

Appendix

On Analytical Conditions for Steady states

State-equations (3.1) can be expressed as a second-order linear differential equation:

$$\frac{d^2\varphi}{dt^2} + 2\alpha\frac{d\varphi}{dt} + \omega_0^2\varphi = \omega\widehat{U}\cos\overline{\omega}t, \quad \alpha = \frac{1}{2RC},\ \omega_0 = \frac{1}{\sqrt{LC}}. \tag{A.1}$$

If $\alpha < \omega_0$, as it is the case for parameter values used in the paper $\overline{C} = 1, \overline{R} = 2, \overline{L} = 5.4$, the solution of the equation can be written as:

$$\begin{gathered}\varphi(t) = K\mathrm{e}^{-\alpha t}\cos(\omega_d t + \theta) + \widehat{\Phi}\cos\left(\omega t - \psi\right),\\ \widehat{\Phi} = \omega\widehat{U}\frac{1}{\sqrt{\left(\omega_0^2 - \omega^2\right)^2 + 4\alpha^2\omega^2}}, \qquad \psi = \operatorname{arctg}\frac{2\alpha\omega}{\omega_0^2 - \omega^2}, \qquad \omega_d = \sqrt{\omega_0^2 - \alpha^2}.\end{gathered} \tag{A.2}$$

The constants K and θ are determined by values of initial conditions, $\varphi(0)$ and $d\varphi/dt|_0$. Equation, (A.1), as well as its solution, (A.2), is valid for the flux reflection model only between the reflections, that is, for flux values $|\varphi| < \Phi_{\mathrm{sat}}$. In the moment t_1 the flux φ reaches the saturation value $\pm\Phi_{\mathrm{sat}}$ and the flux slope $d\varphi/dt$ is alternated, (2.5). After the moment of reflection, the solution, (A.2), is valid again, but through the alternation of flux slope $d\varphi/dt$, the initial conditions are changed and, consequently, the constants of the solution.

Let us denote the solution before the first reflection in moment t_1 as

$$\varphi_1(t) = K_1\mathrm{e}^{-\alpha t}\cos\left(\omega_d t + \theta_1\right) + \widehat{\Phi}\cos\left(\omega t - \psi\right), \quad t_1 > t > 0. \tag{A.3}$$

Table 4: Properties of steady states.

Property (a)	Property (b)	Property (c)	Steady states
$k = 1$	Yes	Yes	Monoharmonic steady state
$k = 1$	Yes	No	Odd higher harmonic steady state
$k = 1$	No	No	Even and odd higher harmonic steady state
$k > 1, k \in N$	No	No	Period-k steady state
$k \to \infty$	No	No	Chaotic steady state

The constants K_1 and θ_1 are determined by given values of initial conditions, $\varphi_1(0)$ and $d\varphi_1/dt|_0$. Generally, the solution after n reflections in moments $t_1, t_2, \ldots, t_{n-1}, t_n$ and before the reflection in moment t_{n+1} is

$$\varphi_{n+1}(t) = K_{n+1}\mathrm{e}^{-\alpha(t-t_n)}\cos\left[\omega_d(t-t_n)+\theta_{n+1}\right] + \widehat{\Phi}\cos\left[\omega(t-t_n)-\psi\right], \quad t_{n+1} > t > t_n > t_{n-1} > \cdots > t_2 > t_1. \tag{A.4}$$

Constants K_{n+1} and θ_{n+1} are determined using the initial conditions $d\varphi_{n+1}/dt|_{t_n}$ and $\varphi_{n+1}(t_n)$, which depend on values of solution $\varphi_n(t)$ and its derivative $d\varphi_n/dt$ in the moment of reflection t_n:

$$\varphi_{n+1}(t_n) = \varphi_n(t_n), \qquad \left.\frac{d\varphi_{n+1}}{dt}\right|_{t_n} = -\left.\frac{d\varphi_n}{dt}\right|_{t_n}. \tag{A.5}$$

Each moment of reflection t_m $(m \in N, t_0 = 0)$ is determined by the condition

$$\left|\varphi_m(t_m)\right| = \Phi_{\mathrm{sat}} \longrightarrow \left|K_m\mathrm{e}^{-\alpha(t_m-t_{m-1})}\cos\left[\omega_d(t_m-t_{m-1})+\theta_m\right] + \widehat{\Phi}\cos\left[\omega(t_m-t_{m-1})-\psi\right]\right| = \Phi_{\mathrm{sat}} \tag{A.6}$$

which cannot be expressed explicitly regarding the moment t_m, that is, moments of reflection can be determined only approximately.

Characteristic steady state is established if the following conditions are met according to Table 4 $(m \in N, t_0 = 0)$:

(a) periodicity:

$$\varphi_m(t_{m-1}) = \varphi_{m+2k-1}(t_{m+2k-1}), \qquad \left.\frac{d\varphi_m}{dt}\right|_{t_{m-1}} = \left.\frac{d\varphi_{m+2k-1}}{dt}\right|_{t_{m+2k-1}}, \qquad t_{m+2k-1} - t_{m-1} = k\frac{2\pi}{\omega}, \tag{A.7}$$

(b) odd-symmetry:

$$\varphi_m(t_{m-1}) = -\varphi_{m+1}(t_m),$$
$$\left.\frac{d\varphi_m}{dt}\right|_{t_{m-1}} = -\left.\frac{d\varphi_{m+1}}{dt}\right|_{t_m}, \qquad t_m - t_{m-1} = \frac{1}{2}\frac{2\pi}{\omega}, \tag{A.8}$$

(c) peak flux value lower as saturation value:

$$\widehat{\Phi} < \Phi_{\text{sat}}. \tag{A.9}$$

However, at the start of transient state, that is, in moment $t = 0$, it is impossible to determine explicitly the ranges of parameter values and values of initial conditions, $\varphi_1(0)$ and $d\varphi_1/dt|_0$, at which a particular steady state would arise because a solution $\varphi_{n+1}(t)$, (A.4), can be obtained recursively only, starting from first solution $\varphi_1(t)$, (A.3), and using approximately determined values of reflection moments $t_1, t_2, \ldots, t_{n-1}, t_n$, (A.6), in each step of recursion.

References

[1] C. Hayashi, *Nonlinear Oscillations in Physical Systems*, McGraw-Hill Electrical and Electronic Engineering Series, McGraw-Hill, New York, NY, USA, 1964.

[2] C. Kieny, "Application of the bifurcation theory in studying and understanding the global behavior of a ferroresonant electric power circuit," *IEEE Transactions on Power Delivery*, vol. 6, no. 2, pp. 866–872, 1991.

[3] B. Lee and V. Ajjarapu, "Period-doubling route to chaos in an electrical power system," *IEE Proceedings: Generation, Transmission and Distribution*, vol. 140, no. 6, pp. 490–496, 1993.

[4] B. A. Mork and D. L. Stuehm, "Application of nonlinear dynamics and chaos to ferroresonance in distribution sysytems," *IEEE Transactions on Power Delivery*, vol. 9, no. 2, pp. 1009–1017, 1994.

[5] S. Mozaffari, M. Sameti, and A. C. Soudack, "Effect of initial conditions on chaotic ferroresonance in power transformers," *IEE Proceedings: Generation, Transmission and Distribution*, vol. 144, no. 5, pp. 456–460, 1997.

[6] M. R. Iravani, A. K. S. Chaudhary, W. J. Giesbrecht, et al., "Modeling and analysis guidelines for slow transients—part III: the study of ferroresonance," *IEEE Transactions on Power Delivery*, vol. 15, no. 1, pp. 255–265, 2000.

[7] J. A. Martinez-Velasco and B. A. Mork, "Transformer modeling for low frequency transients: the state of the art," in *Proceedings of the IPST International Conference on Power Systems Transients*, New Orleans, La, USA, June 2003.

[8] B. A. T. Al Zahawi, Z. Emin, and Y. K. Tong, "Chaos in ferroresonant wound voltage transformers: effect of core losses and universal circuit behaviour," *IEE Proceedings: Science, Measurement and Technology*, vol. 145, no. 1, pp. 39–43, 1998.

[9] D. A. N. Jacobson, P. W. Lehn, and R. W. Menzies, "Stability domain calculations of period-1 ferroresonance in a nonlinear resonant circuit," *IEEE Transactions on Power Delivery*, vol. 17, no. 3, pp. 865–871, 2002.

[10] L. O. Chua, M. Hasler, J. Neirynck, and P. Verburgh, "Dynamics of a piecewise-linear resonant circuit," *IEEE Transactions on Circuits and Systems*, vol. 29, no. 8, pp. 535–547, 1982.

[11] W. L. A. Neves and H. W. Dommel, "On modelling iron core nonlinearities," *IEEE Transactions on Power Systems*, vol. 8, no. 2, pp. 417–425, 1993.

[12] I. Flegar, D. Fischer, and D. Pelin, "Identification of chaos in a ferroresonant circuit," in *Proceedings of the International Conference on Electric Power Engineering (PowerTech '99)*, pp. 1–5, Budapest, Hungary, August-September 1999.